THE JOURNAL OF PHYSICAL CHEMISTRY B
A JOURNAL OF THE AMERICAN CHEMICAL SOCIETY

pubs.acs.org/JPCB

Article

Influence of Polarizability on the Structure, Dynamic Characteristics, and Ion-Transport Mechanisms in Polymeric Ionic Liquids

Zidan Zhang, Everett Zofchak, Jakub Krajniak, and Venkat Ganesan*

Cite This: *J. Phys. Chem. B* 2022, 126, 2583−2592

Read Online

ACCESS | Metrics & More | Article Recommendations | Supporting Information

ABSTRACT: We used atomistic simulations and compared the prediction of three different implementations of force fields, namely, the original full partial charge system, the scaled partial charge system, and the Drude oscillator polarizable force field and its effect on the structural and dynamic properties of a polymeric ionic liquid, poly(1-butyl-3-methyl-imidazolium hexafluorophosphate). We found that both the scaled and the polarizable force field models yield comparable predictions of structural and dynamic properties, although the scaled charge model artificially lowers the first-neighbor peak of the radial distribution function and therefore leads to a slight reduction in density. The full charge model was not accurate in its prediction of the dynamic properties but could reproduce the structural properties. With a refined analysis method for the ion-hopping mechanisms, we found that all three methods produce very similar conclusions, namely, that the mobile anion is associated with three cations from two distinct polymer chains and that the fractions of inter- and intramolecular hopping events are comparable. Our results demonstrate that the scaled charge force fields provide a computationally efficient means to capture polarizability effects on both the structural and dynamic properties of polymeric ionic liquid systems.

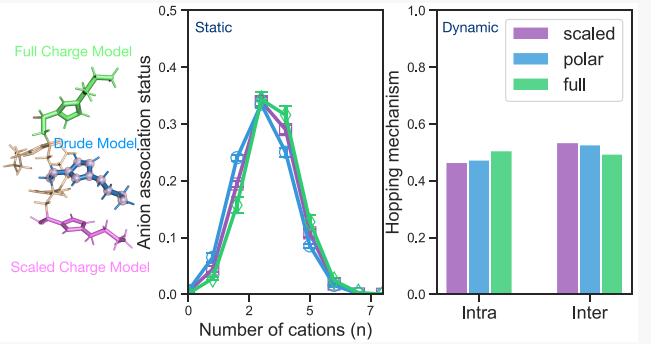

1. INTRODUCTION

Lithium ion batteries (LIBs) are finding widespread use in a variety of day-to-day applications such as mobile phones and electric vehicles.[1−4] Despite the promise, it has been found that the LIBs exhibit problematic issues related to flammability, liquid electrolyte leakage, dendrite formation, low thermal stability, poor mechanical properties, and toxicity.[5] Solid polymer electrolytes (SPEs) have been proposed as one potential candidate for alleviating some of the issues plaguing the electrolytes in LIBs.[6−13] As a family member of SPEs, polymeric ionic liquids (polyIL) exhibit the attractive combination of physicochemical and ion-transport characteristics of ILs and enhanced mechanical properties of polymers.[14−16] As a result, such materials exhibit high conductivities and lower glass-transition temperatures even at high charge densities. Consequently, polyILs have attracted considerable interest as potential electrolytes for LIBs.[17−25]

In our previous studies, we have used nonpolarizable atomistic molecular dynamics simulations to study the ion-transport mechanisms in polyILs and related systems, such as the origin of the ion-transport mechanism;[26] the influence of the polymer chain length, types of counterions, and morphology on the ion-transport mechanism;[27−31] the influence of the lithium salt concentration or monomeric ionic liquid concentration on the ion-transport mechanisms;[32−35] and the influence of ion correlations on the inverse Haven ratio.[36] As has been common practice, the lack of polarizability effects was compensated for by a simple charge scaling of the charged groups.[28,29,33,37,38] Our studies demonstrated that ion transport in such systems is governed by a hopping process involving ion pair association/dissociation of the mobile ion associated with counterions from distinct polymer chains. Such simulations were used to rationalize a number of experimental observations relating to the behavior of conductivity in simple homopolymeric polyILs,[26−31,36] diblock copolymeric polyILs,[30,31] and salt-doped polyILs.[32−35]

More recently, significant interest has arisen with respect to the influence of polarizability on the structure and dynamics of soft matter systems.[39−46] Broadly, there are three primary methods for explicitly accounting for the effects of electronic polarization in classical simulations, namely, the induced point dipole, fluctuating charge, and the Drude oscillator models.[39,47,48] The total electrostatic energy of the induced point dipole system contains the charge−charge, charge−dipole, and dipole−dipole interactions, with the point dipole on a given atom calculated using an iterative self-consistent field (SCF)

Received: December 18, 2021
Revised: March 14, 2022
Published: March 29, 2022

https://doi.org/10.1021/acs.jpcb.1c10662
J. Phys. Chem. B 2022, 126, 2583−2592

procedure.[49−54] The fluctuating charge model allows the charges on individual molecules to dynamically change according to the electronegativity of each atom in the molecule.[55−60] The Drude oscillator model attaches a ghost (Drude) particle to its host (core) particle with a harmonic spring, and then the mass and partial charge of the true atom are divided into the Drude and core portions.[39,54,61−66] In general, in comparison to the traditional nonpolarizable force field (fixed charge) model, all of the polarizable models introduce additional degrees of freedom to be solved self-consistently during the simulation, which increases the computational expense and serves to explain the relatively fewer number of studies employing such a framework.

Recently, Maginn et al. compared the prediction of structural, thermodynamic, and transport properties of molten salt by using fixed-charge and induced-dipole models for polarizability.[67] They found that both models predict similar structural and dynamic properties of multiple types of molten salts, with the only property exception being the liquid density, where the induced-dipole model yielded more accurate results. McDaniel et al. studied the influence of electronic polarization on the structural properties of ionic liquid systems.[68] Upon systematically comparing the ion pair interactions (anion−anion, anion−cation, and cation−cation) between the fixed-charge model and polarizable model, they found that the ion pair interactions are more repulsive and more localized in the absence of polarization. Pádua et al. suggested that the scaled-charge model would artificially lower the first-neighbor peak and therefore predict a lower density in comparison to experimental values.[69] Besides the structural and dynamic properties, the influence of polarizability on the phase behavior has also been probed in recent studies.[70,71]

Motivated by the above studies, in this article we revisit and present results for the influence of polarizability on the structure and ion-transport mechanisms in polymeric ionic liquids. Specifically, we compare the predictions of three different implementations of the force field, namely, the original full partial charge (FC) system, the scaled partial charge (SC) force fields, and the Drude oscillator polarizable force field (PF) on the structural and dynamic properties of the polyIL poly(1-butyl-3-methyl-imidazolium hexafluorophosphate). We find that both the scaled and the polarizable force field models produce comparable predictions of structural and dynamic properties. However, the scaled charge model artificially lowers the first-neighbor peak of the radial distribution functions (between anion and cation) compared to the polarizable force field and therefore leads to a slight reduction in density. (In SI Section S1, we show the mass density of the investigated systems.) In contrast, the full partial charge model was found to be inaccurate for the prediction of the dynamic properties, but it could reproduce the structural properties. With a refined approach for probing ion-hopping mechanisms, we found that all three methods produce very similar conclusions, namely, that the mobile anion is associated with three cations from two distinct polymer chains and that the fractions of inter- and intramolecular hopping events are comparable. Together, our results suggest that the scaled partial charge approach provides an efficient computational approach to accommodate much of the physics arising from polarizability characteristics.

The rest of this article is organized as follows. In section 2, we describe the implementation details of the nonpolarizable force field model and the polarizable force field. In section 3, we discuss the results of mobile ion diffusion coefficients, the static ion pair association status, and the anion transport mechanisms. We conclude with a brief summary of our findings and conclusions in section 4.

2. SIMULATION DETAILS

2.1. Nonpolarizable Force Field Model. In the present study, we used atomistic molecular dynamics simulations to investigate the structural and dynamic properties of poly(1-butyl-3-methyl-imidazolium hexafluorophosphate) ($[BmIm]^+[PF_6]^-$). The setup of the simulated system is the same as in our initial study,[26] where the polymer chain length is 32, the number of chains is 8, and the total number of ion pairs is 256. The all-atom optimized potential for liquid simulations (OPLS-AA) was employed to model the bond, angle, dihedral, improper torsions, and nonbonded interactions,[72] and the potential energy of the system can be described using the following function:

$$U(r) = U^{\text{bond}}(r) + U^{\text{angle}}(\theta) + U^{\text{dihedral}}(\phi) + U^{\text{improper}}(\psi) + U^{\text{nonbonded}}(r) \quad (1)$$

In eq 1, the first two terms were modeled using the harmonic function form, the dihedral potential adopted the Fourier function form, the improper torsion employed the periodical function form, and the nonbonded interactions could be written as

$$U^{\text{nonbonded}}(r) = \sum_{i}^{N}\sum_{j>i}^{N} f_{ij}\left[4\epsilon_{ij}\left[\left(\frac{\sigma_{ij}}{r_{ij}}\right)^{12} - \left(\frac{\sigma_{ij}}{r_{ij}}\right)^{6}\right] + \frac{q_i q_j e^2}{r_{ij}^2}\right] \quad (2)$$

In eq 2, f_{ij} was used to scale 1−4 interactions by a factor of 0.5, the interactions beyond 1−4 interactions were not influenced, and f_{ij} was set to 1.0. The pairwise Lennard-Jones (LJ) parameters (ϵ and σ) and the partial charges were explicitly listed in our recent papers[26] (and are listed in SI Section S2), and the geometric combining rule was used to generate the LJ parameters for cross-terms. The optimized partial charges were used directly for the full partial charge FC system. For the scaled partial charge system, a factor of 0.8 was applied to scale the partial charges. Such a factor that has been suggested in past studies has yielding better agreement between the dynamic properties obtained from the simulations and the experiments.[28,29,33,37,38,73]

The initial configuration of the simulation box was constructed by packing eight polymer chains randomly into the simulation box by Packmol.[74] A multistep pre-equilibration scheme inspired by the 21-step decompression method proposed by Colina and co-workers was used to decompress the initial simulation box to the experimental densities.[75,76] A single loop of the multistep pre-equilibration consists of three steps: (i) 0.1 ns NVT simulation at 1000 K, (ii) 0.1 ns NPT simulation at 600 K and 100 bar, and (iii) 0.1 ns NPT simulation at 600 K and 1 bar. In our study, such a loop was repeated eight times. The configuration that was obtained from the above pre-equilibration procedure was used for the production run with the NPT ensemble for 220 ns, and the last 200 ns trajectories were used for analyzing the statistical and dynamic properties.

The force, velocity, and position of the simulations were updated with the time step δt = 1 fs. The cutoff for 12−6 Lennard-Jones potential was set to 1.2 nm, and the long-range electrostatic interactions were calculated with the particle−

https://doi.org/10.1021/acs.jpcb.1c10662
J. Phys. Chem. B 2022, 126, 2583−2592

particle particle−mesh (PPPM) solver with a tolerance of 1×10^{-5}. The Nosé−Hoover thermostat was used for temperature coupling at 600 K, and a Parrinello−Rahman barostat was used for pressure control at 1 atm, with the corresponding coupling parameters $\tau_T = 0.2$ ps and $\tau_P = 0.5$ ps. The choice of 600 K as the temperature for our simulations was to ensure that we could extract meaningful displacement statistics for anion transport.[27] Five samples with different initial configurations were used to average the presented statistical and dynamic properties. The centers of mass of the imidazolium $[BmIm]^+$ and anion $[PF_6]^-$ were used for the analysis of the radial distribution functions and the dynamic properties. All of the all-atom simulations were performed with the large-scale atomic/molecular massively parallel simulator (LAMMPS),[77] the source code was downloaded from the official repository on Github, and the patch date of the compiled version was May 14, 2021.

2.2. Polarizable Force Field Model. In the current study, we employed the Drude oscillator model developed by Pádua et al.[69,78] to account for the effects of polarizability. In Pádua's approach, the mass of the Drude particle was fixed as 0.4 au, the spring constant (k_D) for the harmonic potential between the Drude and core particles was 4184 kJ·mol^{-1}, and the equilibrium bond distance of the harmonic potential was 0.0 nm. The partial charge (q_D) on the Drude particle was calculated using

$$q_D = (\alpha k_D)^{1/2} \tag{3}$$

where α is the atomic polarizability obtained from the literature.[79] We note that only heavy atoms are considered to be core particles, and the polarizabilities of the hydrogen atoms are merged into their corresponding heavy atoms. The summations of the masses and charges of the Drude and core particles were equal to the mass and charge of the original atom.

At short distances, the electrostatic interactions between the neighboring Drude particles could lead to instabilities in the simulation. To alleviate this issue, the Thole damping function with a universal damping parameter (a = 2.6) was utilized to reduce the electrostatic interactions.[80,81] Because of the additional degrees of freedom that were induced by the Drude particles, the temperature-grouped Nosé−Hoover thermostat was used for the temperature coupling of the core particles at 600 K and of the Drude particles at 1 K.[82] All other settings that control the molecular dynamics simulation as well as the pre-equilibration and production procedures were the same as that in the nonpolarizable force field simulation. The polarizable force field simulation with the Drude oscillator model can be enabled in LAMMPS by activating the USER-DRUDE package[69] (the date of the compiled version was the same as above).

2.3. Performance Benchmark. As has been mentioned above, the introduction of the Drude particles would introduce an additional degree of freedom into the computations and thereby increase the cost of the simulations. All of the simulations were performed at the Texas Advanced Computing Center (TACC). The CPU is an Intel Xeon Platinum 8280 (Cascade Lake) which has 56 cores on two sockets with a 2.7 GHz clock rate, and the RAM is DDR4 with a 192 GB capacity. The fixed-charge systems could compute 1.24 ns (scaled charge) and 1.19 ns (full charge) per hour per computing node. In contrast, the system with a polarizable force field could compute only 0.25 ns per hour per computing node, which is about 5 times slower than that of the fixed-charge systems.

3. RESULTS AND DISCUSSIONS

The fully charged OPLS-AA force field (FC) is parametrized to accurately describe the physical properties (such as density, heats of vaporization, and structural properties) of the modeled systems. However, in such force fields, dynamic properties such as the diffusivity of ions are often underestimated relative to experiments. A popular solution to address the underestimated ion-transport properties using the traditional fixed-charge model is to apply a scale factor to the point partial charges (SC force field). Several studies have demonstrated that the structural and physical properties can still be captured by applying a charge-scaling factor of 0.7−0.9, whereas the transport properties are displayed better in comparison to the experiments.[28,29,33,37,38,73] However, to our knowledge, in the context of polyILs, there has not been a comparison of whether the scaled charges capture the structure and dynamic properties of the polarizable force fields (PF). More generally, while the SC system reduces the electrostatic interactions and accelerates the dynamics, it is not clear if the specific mechanisms of ion transport can also be captured in such a simplistic approach. The results below present such an explicit comparison while simultaneously examining the performance of the fully charged force field.

Ion Diffusivity. To compare the influences of different implementations of the force fields on the ion transport in polymeric ionic liquid, we first examine the predictions for the anion (the mobile ion) diffusivity arising in the different models.

The mean square displacements (MSDs) for the PF_6^- anion as well as their corresponding fits are shown in Figure 1. In

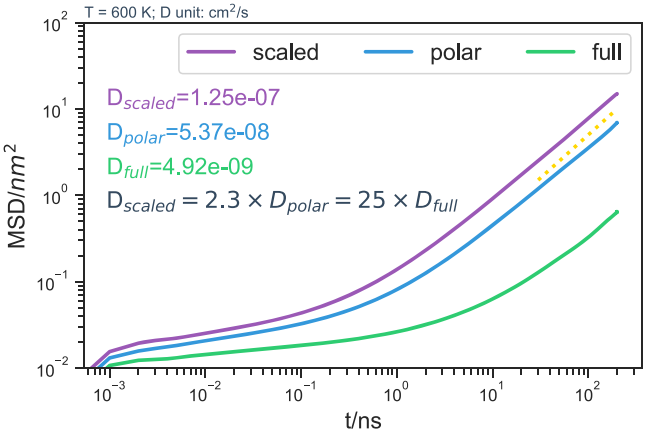

Figure 1. Mean square displacements for a nonpolarizable force field with scaled charges (scaled), the polarizable force field (polar), and the nonpolarizable force field (full). The yellow dotted line is the benchmark line indicating the diffusive region, which has a slope of 1.0 on the log−log scale.

Figure 1, we can immediately see that the MSD of the SC system is faster than those of the PF and FC systems. However, the MSD of the PF system is seen to be closer to that of the SC system compared to that of the FC system. The fitted D_{polar} and D_{full} values are about 5.37×10^{-8} and 4.92×10^{-9} cm^2·s^{-1}, which are factors of 2.3 and 25 times smaller than D_{scaled}, respectively (the linear fitting of the corresponding MSDs is shown in SI Section S3). We note that the fitted D_{scaled} value is about 1.25×10^{-7} cm^2·s^{-1}, which is smaller than the diffusivity (1.70×10^{-7} cm^2·s^{-1}) reported for polyILs with a polymer chain length of 8 in our other study.[30] These differences in D_{scaled} can be explained by the fact that the diffusion coefficient decreases with increasing

https://doi.org/10.1021/acs.jpcb.1c10662
J. Phys. Chem. B 2022, 126, 2583−2592

polymer chain length[27] and that the polymer chain length in the present study is 32.

The above results suggest that the anion diffusion is almost an order of magnitude slower in the full charge (FC) model than in the PF model. By simply applying a uniform scale factor (0.8 in the current study), the anion diffusion coefficient significantly improves in comparison to the PF system. However, it can also be seen that a scaling factor of 0.8 may not universally capture the diffusion coefficient of PF with quantitative accuracy. Instead, our results indicate that the actual scaling factor may have to be tuned to the specific system under consideration.

Cohesive Energy. The cohesive energy of the polyIL, which is the difference between the energy of the polyIL and the isolated ions (polycations and anions), is calculated to validate the correctness of the adopted force fields.[68,83,84] The cohesive energy E_{coh} is evaluated through the expression

$$\langle E_{coh}\rangle = \langle E_{total}\rangle - \langle E_{+}\rangle - \langle E_{-}\rangle \tag{4}$$

where $\langle E_{total}\rangle$ is the total energy (normalized by the number of ion pairs) and $\langle E_{+}\rangle$ and $\langle E_{-}\rangle$ are the energies of the polycation and anion in the gas phase, respectively. $\langle\cdots\rangle$ represents the ensemble average over the MD trajectories. (The details for calculating the cohesive energy in the gas phase are described in SI Section S4.)

The calculated E_{coh} values for different force fields are summarized in Table 1. From the values, we can see that the E_{coh} for the SC model is about 33% lower than the E_{coh} for the FC model, in agreement with the expectation that the SC model cannot accurately predict the cohesive energy in a monomeric ionic liquid system,[83] although the SC model is cost-effective and is semiquantitatively accurate in its prediction of the diffusion coefficient. The E_{coh} for the PF model is about 10% lower than the E_{coh} for the FC model. The corresponding deviation is about 5% between the nonpolarizable and polarizable force fields for 1-butyl-3-methyl-imidazolium tetrafluoroborate ($[BmIm]^+[BF_4]^-$) that was optimized using the first principles method,[83] and the deviation was about 0.2 to 13.1% for multiple monomeric ionic liquids (cf. Table 2[69]) that used the same polarizable implementation as ours.

Table 1. Comparison of Density and Cohesive Energy at 600 K for a Nonpolarizable Force Field with Scaled Charges (SC), the Polarizable Force Field (PF), and the Nonpolarizable Force Field (FC)

	E_{coh} (kcal·mol^{-1})	ρ (kg·m^{-3})
scaled	−161.64246	1.20437
polar	−216.56906	1.25280
full	−240.71630	1.27576

Furthermore, the densities of three systems are also reported in Table 1. Therein, we can see that the trend in the density is the same as what we saw for the cohesive energy, meaning that the density for the SC model is the lowest, which is about 5.6% lower than that for the FC model. The deviations between the FC model and the SC model were about 1.5 to 6.1% for 29 types of monomeric ionic liquid in Acevedo and associates' work.[85] The predicted density of the PF model is about 1.8% lower than that of the FC model. The above results indicate that the SC model underestimates both the cohesive energy and the density. In contrast, the predictions of the cohesive energy and density of the PF model are comparable to those of the FC model.

Structural Characteristics of Ions. We characterized the structural features of the different systems through the radial distribution function for anion−cation pairs

$$g_{ij}(r) = \frac{V}{N_i N_j}\left\langle \sum_{i=1}^{N_i}\sum_{j=1}^{N_j}\frac{\delta(r_{ij}-r)}{4\pi r^2}\right\rangle \tag{5}$$

where N_i and N_j are the number of atoms of polycation $BmIm^+$ and anion PF_6^-, V is the time-averaged volume of the simulation box, and δ is the Dirac delta function. For the polycation $BmIm^+$, we chose the center of mass of the imidazolium to represent the reference, and for the anion PF_6^-, we also used the center of mass as the reference. (In SI Section S5, we use the carbon atom on the N−C−N bridge to represent the $BmIm^+$ polycation and the phosphorus atom to represent the PF_6^- anion.)

The calculated $g(r)$ values for the three force fields are shown in Figure 2. Figure 2a,b displays the $g(r)$ for the like-ion species. It is seen that the different force field models have only a limited influence on the anion−anion ion pair interactions. In contrast, the cation−cation interactions are significantly impacted by different models. Explicitly, the PF model has higher ion-pair interactions than the other two models. Such results indicate that the induced Drude particles and the changes in the charges for the core particles have a significant impact on the ion pairing of the connected (due to the backbone) polycations.

The inset of Figure 2c displays the magnified $g(r)$ that contains the information on the main peak for the anion−cation interaction, where we can see that the SC system has the smallest peak intensity. Furthermore, we observe that the cutoff which determines the first solvation shell (i.e., the location where $g(r)$ = 1.0 after the first peak) is the largest (0.63 nm) for the scaled charge system in comparison to the other two systems, while the cutoffs for the polar system and the full partial charge system are almost identical (0.61 nm). Such results support the reasoning that the weaker anion−polycation interactions in the SC system facilitate faster anion transport in such cases.[69] More interestingly, in comparing the predictions of the FC and SC models to PF, the peak intensity and the first solvation shell are seen to be more accurately reflected in the FC model. Such results again reinforce that whereas the SC model artificially decreases the interaction between the anion and polycation to capture the polyIL dynamic characteristics, such features come at the expense (albeit, small) of an accurate prediction of the structural characteristics.

Furthermore, the charge oscillations in the different force fields were also probed. The latter is related to the net-neutrality condition,[84]

$$\int_0^{\infty}\frac{4}{3}\pi r^2\left[\sum_{\alpha} q_\alpha \rho_\alpha g_{\alpha\beta}(r)\right]\mathrm{d}r = -q_\beta \tag{6}$$

where α and β are either polycation $BmIm^+$ or anion PF_6^-, q is the anion charge, ρ is the number density, and $g(r)$ is the radial distribution function. Instead of extending the limits to infinity, a distance-dependent summation has been calculated since the simulation box would have an actual finite size:

$$\int_0^{r}\frac{4}{3}\pi r^2\left[\sum_{\alpha} q_\alpha \rho_\alpha g_{\alpha\beta}(r)\right]\mathrm{d}r = -q_\beta^{\mathrm{sum}}(r) \tag{7}$$

The calculated charge oscillations are displayed in Figure 2d, wherein it can be seen that q_{sum} for polycation $BmIm^+$ (dark gray) and anion PF_6^- (purple) fluctuates and decays around −1

https://doi.org/10.1021/acs.jpcb.1c10662
J. Phys. Chem. B 2022, 126, 2583−2592

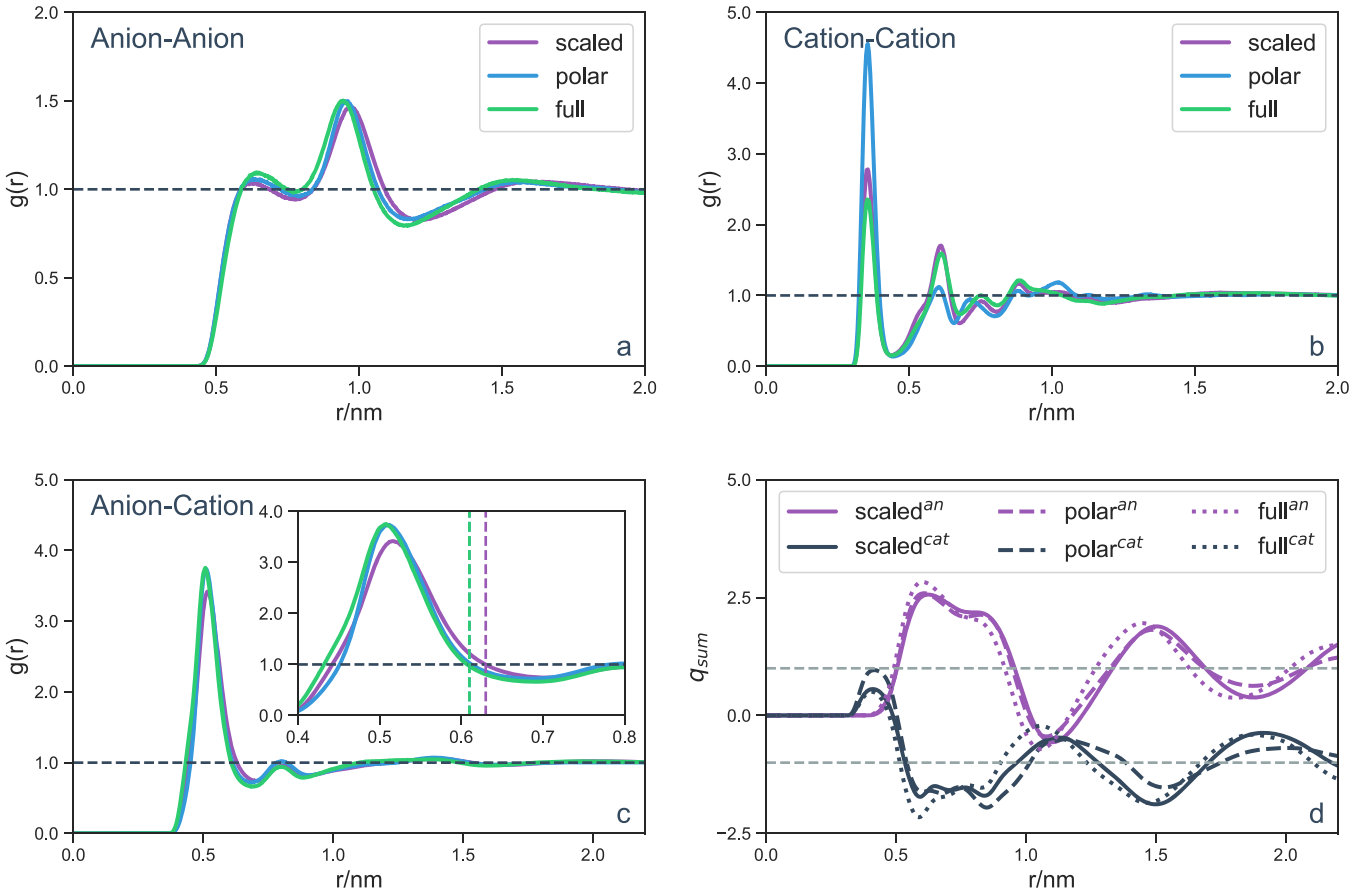

Figure 2. Radial distribution functions ($g(r)$) for the nonpolarizable force field with scaled charges (scaled), the polarizable force field (polar) and nonpolarizable force field (full) for (a) anion−anion, (b) cation−cation, (c) anion−cation, and (d) the charge oscillation for anion and cation.

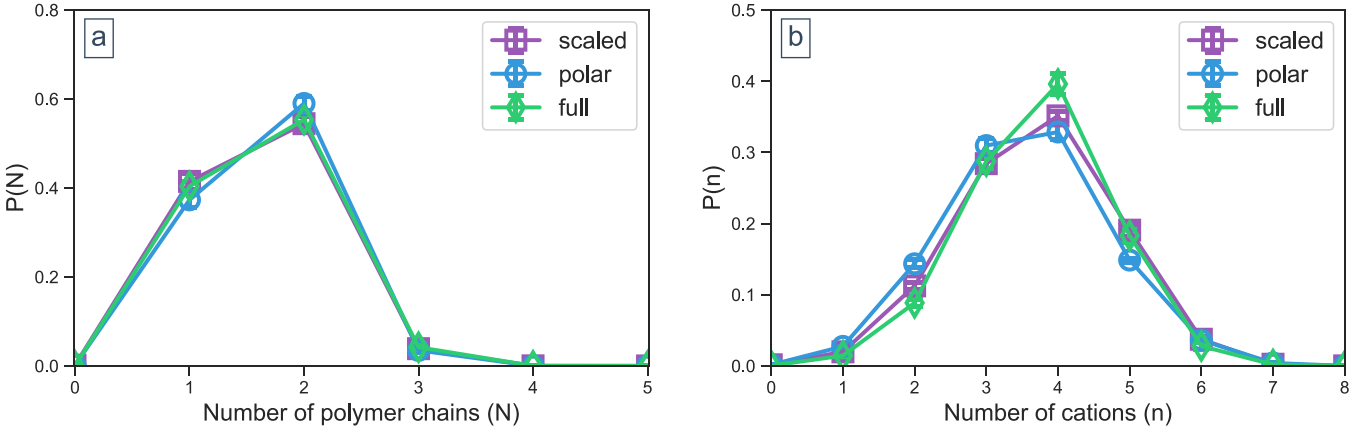

Figure 3. (a) Probability that a given anion is associated with N polymer chains $P(N)$. (b) Probability that a given anion is associated with n cations $P(n)$.

and 1, respectively, indicating the satisfaction of the net-neutrality condition. It is worth mentioning that the PF model has smaller long-range charge oscillations, which is consistent with the Stillinger−Lovett sum rule and further demonstrated that the lack of electronic polarization effects would influence the prediction of long-range ion structure.[84]

In addition, the influence of different force field models on the polymer structure has been probed by calculating the radius of gyration R_g. The calculated R_g values for the SC, PF, and FC models are 2.02, 1.99, and 2.05 nm, respectively. Although the results for $g(r)$ for cation−cation and q_{sum} for the cation indicate that the influence of polarizability is not negligible, the influence on the polymer structural features such as R_g is seen to be minimal.

Ion-Transport Mechanisms. One of the objectives of the present study is to go beyond a comparison of simple structural measures such as $g(r)$ and instead more directly probe the influence of polarizability on the mechanisms of ion transport and especially the ability of the SC model to capture such details. In our previous studies with the SC model, we have shown that, at equilibrium, the mobile ion prefers to associate with four counterions that are from two distinct polymer chains.[26−33]

https://doi.org/10.1021/acs.jpcb.1c10662
J. Phys. Chem. B 2022, 126, 2583−2592

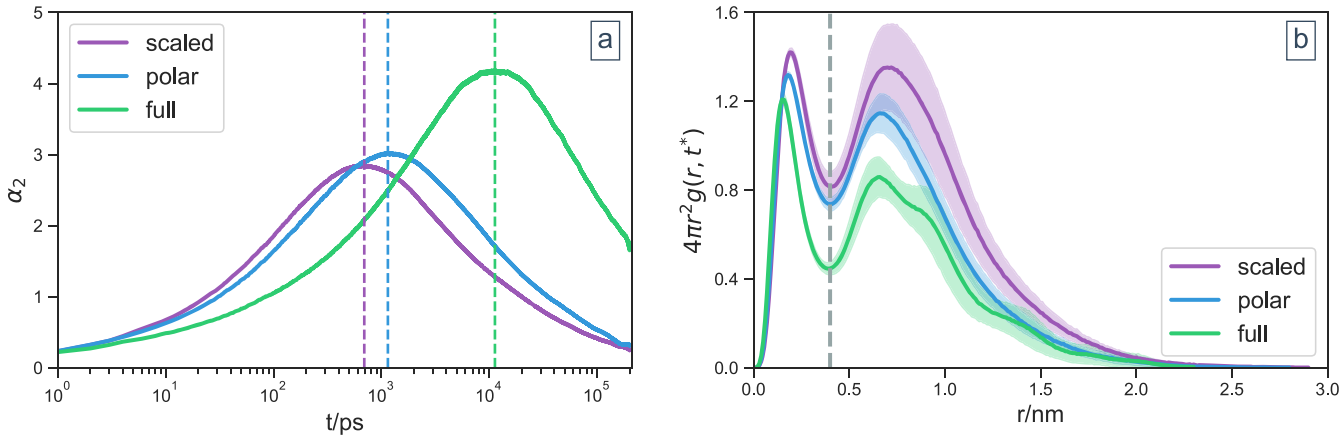

Figure 4. (a) Non-Gaussian heterogeneity parameter α_2 (the vertical line indicates the position where α_2 reaches the maximum) and (b) the self-van Hove function at t^* that was obtained from the maximum in α_2.

Furthermore, the accompanying ion-transport process was shown to retain such static features and was governed by the association/dissociation events involving intra- and intermolecular hopping processes.

For the present study, in Figure 3 we display the results for the probability distribution that a given anion is associated with N polymer chains $P(N)$ and n polycations $P(n)$. As can be seen from the probability distributions, we observe very similar features for both $P(N)$ and $P(n)$ among all three different implementations of force field models. Explicitly, a maximum of $P(N)$ at $N = 2$ is observed in Figure 3a, indicating that a given anion is preferentially associated with two distinct polymer chains. Furthermore, a maximum of $P(n)$ at $n = 4$ can be seen in Figure 3b, suggesting that a given anion is likely to associate with four polycations. Such results agree with our previous studies[26−33] and suggest that the different implementations of the force field have very limited influences on the ion-pair association distributions.

To complete the characterization and comparison of anion-transport mechanisms, we adopt an approach different from our earlier studies. To recall, in our previous studies, we utilized two types of ion-hopping analysis, namely, the ion-pair-based analysis[30] and the mobile-ion-centered analysis.[26] The common feature of such analyses is the use of the instantaneous association status of ion pairs to determine whether an ion has executed a hopping event between time frames of observation. A recent study by Paddison et al.[86] demonstrated that characterizing ion-hopping mechanisms based on neighboring frame analysis typically overcounts the movements due to not discounting ion-rattling events.[34] Instead, Paddison et al. have used an approach based on the self-van Hove function to quantify temporal and spatial hopping events,[86] which enables the filtering of the rattling or ineffective hopping events. The idea behind such methodology is to use the self-van Hove function to first identify the time scale (t^*) beyond which an ion can be deemed as moving further from its cage (i.e., rattling). Subsequently, the analysis considers only ions which move beyond the critical distance (r^*) encompassing the length scale of the cage to identify "truly" mobile ions and the mechanisms of their motion.

To implement the refined ion-hopping analysis (in SI Section S6 we discuss the results of the hopping event analysis based on the original neighboring frame approach), two system-dependent parameters should be defined prior to the hopping analysis, namely, the critical temporal parameter t^* and the critical spatial parameter r^*. The critical time t^* can be defined as the transition point from the subdiffusive regime to the diffusive regime and can be obtained by considering the non-Gaussian heterogeneity parameter $\alpha_2(t)$ defined as

$$\alpha_2(t) = \frac{3\langle (r(t) - r(0))^4 \rangle}{5\langle (r(t) - r(0))^2 \rangle^2} \tag{8}$$

where $r(0)$ and $r(t)$ are the particle position at reference time $t = 0$ and current time t, respectively, and $\langle \cdot \rangle$ represents the ensemble average. The results of non-Gaussian heterogeneity parameter α_2 for three systems are shown in Figure 4a. The location of the maximum in α_2 indicates the transition point from the subdiffusive regime to the diffusive regime, and the corresponding time t is taken as the critical time t^*. We observe that the scaled partial charge system exhibits the fastest t^* (693 ps). The t^* of the polar system is close to the scaled partial charge system (1147 ps), and the full partial charge system exhibits the slowest t^* (11 277 ps). Such results are consistent with the hierarchy and orders of magnitude of the diffusion coefficients obtained using the different force fields.

After obtaining the critical time t^*, we then evaluate the self-van Hove function to find the critical distance r^* characterizing a hopping event. The self-van Hove function $4\pi r^2 g(r, t)$ is a function that describes the probability of finding a particle at time t a distance r from its original position. Figure 4b displays the self-van Hove function of three systems at their corresponding critical time t^*. In all cases, we observe two peaks in the probability distribution. The first peak signifies the rattling motion of the ions inside the ballistic cage, whereas the second portion indicates the probability of anions which have hopped to their new positions. (In SI Section S7, we show that the new position corresponds to the length of first solvation shell.) We adopt the position of the valley between the two peaks as the critical length r^*. In other words, an anion is considered to be truly participating in a hopping event only if it travels further than r^* in time t^*. It can be observed that although different force fields exhibit different critical times t^*, the critical lengths r^* are aligned at the same value of 0.4 nm. Such results are again consistent with the fact that the different implementations of force fields displayed only minor differences in structural properties despite exhibiting very different dynamic characteristics.

https://doi.org/10.1021/acs.jpcb.1c10662
J. Phys. Chem. B 2022, 126, 2583−2592

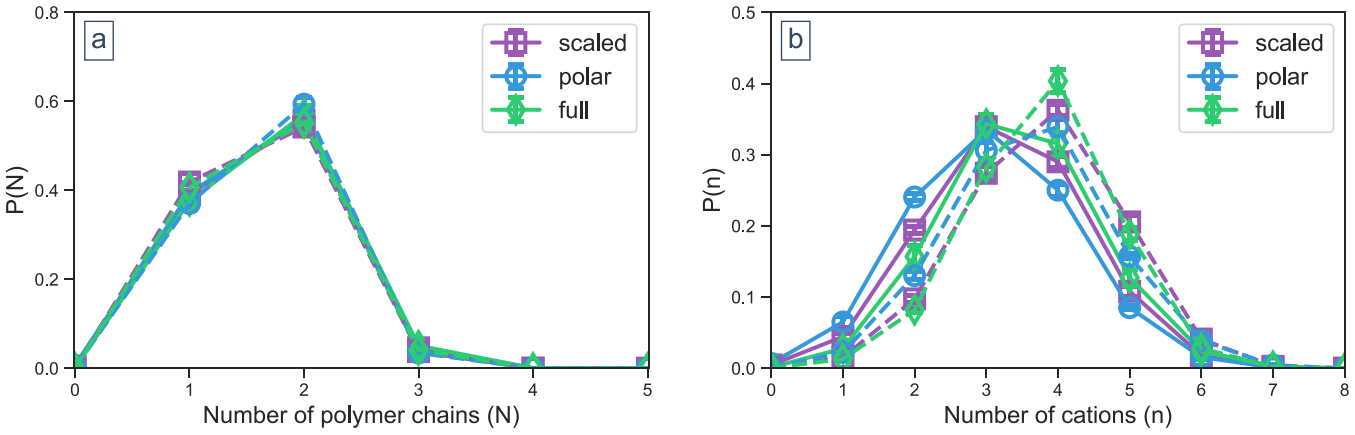

Figure 5. (a) Probability that a given anion is associated with the number of polymer chains $P(N)$ and (b) with the number of cations $P(n)$, where the solid line represents the mobile ions and the dashed line represents the immobile ions.

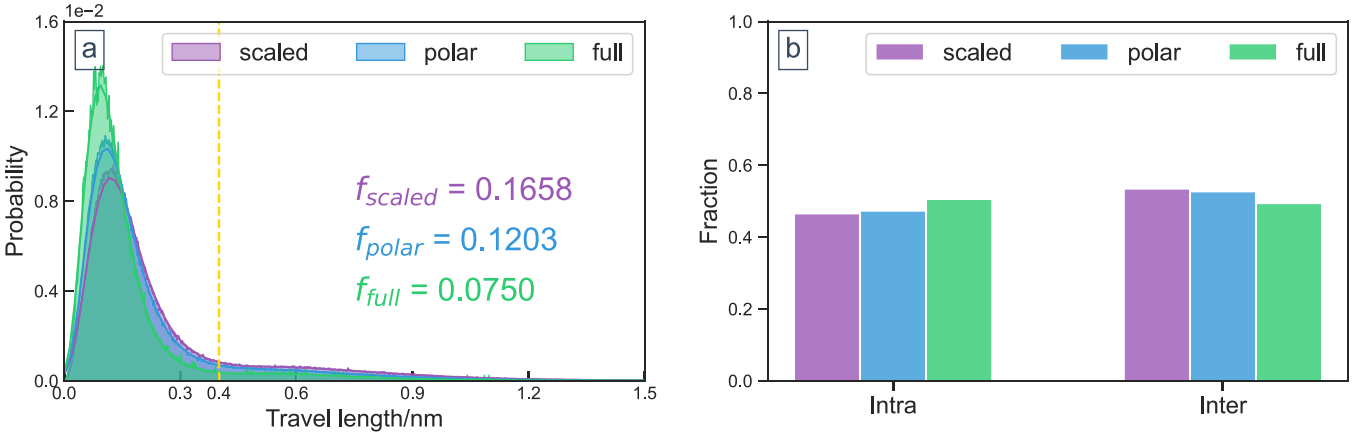

Figure 6. (a) Distribution probability of the travel length of all anions at time t^* and (b) the intra- and intermolecular hopping fractions only for anions that could travel farther than r^* = 0.4 nm.

On the basis of the identification of the mobile ions, we revisit the ion pair association distributions in order to characterize the status of the mobile ions prior to the actual hopping event. From the results displayed in Figure 5a we can see that there are no significant differences in the anion-chain association when compared to the distributions displayed by all of the anions (Figure 3a). Specifically, we still observe a maximum of $P(N)$ at $N = 2$, suggesting that both the mobile and immobile anions prefer to associate with two distinct polymer chains. Furthermore, the choice of the force field seems to have very little influence on the probability distributions of the anion-chain associations. However, the ion pair associations are quite different between the mobile and immobile anions, as shown in Figure 5b. Explicitly, a maximum of $P(n)$ at $n = 3$ can be observed for the mobile anions, which contrasts with a maximum of $P(n)$ at $n = 4$ seen for the immobile anions. Such results suggest that an ion pair association has to be lost to facilitate a successful hopping event of an anion.

In comparing the different force fields, we do observe noticeable differences among the probability distributions. Specifically, the PF system displays a broader distribution of coordination for the mobile ions with a higher fraction of ions being coordinated with only two cations before the hopping events. In contrast, the FC system displays a larger fraction of ions being coordinated with four cations before the hopping event. While such results do not lend themselves to a simple physical explanation, we expect such characteristics to play a role in the dynamic correlations between the ions and the quantitative values of conductivities predicted by the different force fields.

Next, using both the temporal scale t^* and the spacial scale r^*, we quantify the anion-hopping mechanisms and probe the influence of different implementations of force fields. In Figure 6a, we display the probability distribution of the travel length of all anions at the critical observation time t^*, where we see that there is a strong peak in the short travel length range ($r < r^*$), which indicates that a considerable number of anions are just rattling within their ballistic cages. By integrating the probability distribution for $r > r^*$, we can obtain the fraction of anions which are truly "mobile." From the results displayed in Figure 6a, we observe that the fractions of mobile ions mirror the trends observed in the dynamic characteristics, viz., $f_{scaled} \simeq 17\% > f_{polar} \simeq 12\% > f_{full} \simeq 7.5\%$.

On the basis of the identification of the mobile ions, we quantify the fraction of inter- and intramolecular hopping events. Explicitly, subsequent to ion hopping, if the newly formed ion pair retains its original polymer chain identity, then the event is viewed as an intramolecular hopping event. In contrast, if the newly formed ion pair involves a new polymer chain identity, then the event is categorized as intermolecular hopping. From the results displayed Figure 6b, the fractions of intra- and intermolecular hopping are seen to be comparable for

https://doi.org/10.1021/acs.jpcb.1c10662
J. Phys. Chem. B 2022, 126, 2583−2592

all three systems, with the fractions being about 50%. It is observed that the SC system displays a slightly larger extent of intramolecular hopping in comparison to the PF case. The FC case not only exhibits the largest extent of intramolecular hopping but also suggests (in contradiction with the PF results) that the intramolecular hopping events are dominant compared to the intermolecular events. Although the SC case underpredicts the extent of intramolecular events relative to PF, the former does seem to capture the dominant nature of the intermolecular hopping events.

4. CONCLUSIONS

In this study, we presented the results of atomistic simulations comparing the predictions of three different implementations of force fields, namely, the original full partial charge system, the scaled partial charge system, and the Drude oscillator polarizable force field, for the structural and dynamic properties of a polymeric ionic liquid, poly(1-butyl-3-methyl-imidazolium hexafluorophosphate). Our results demonstrate that both the scaled and polarizable force field models are comparable in their predictions of structural and dynamic properties, although the scaled charge model artificially lowers the first-neighbor peak of the radial distribution function. The full charge model was not accurate in its prediction of the dynamic properties but could reproduce the structural properties. With a refined analysis method for the ion-hopping mechanisms, we found that all three methods produce very similar conclusions, namely, that the mobile anion is naturally associated with three cations from two distinct polymer chains and that the fractions of inter- and intramolecular hopping events are comparable.

Together, our results demonstrate that the scaled charge force fields do serve to provide a computationally efficient means to capture polarizability effects for both the structural and dynamic properties of polymeric ionic liquid systems. In future studies, it would be of interest to determine if higher-order dynamic features such as dynamic ion correlations are also equally well reflected in the scaled charge models. Such measures are of interest in accurately computing quantities such as the conductivity[87] and transference number.[36,88,89]

■ ASSOCIATED CONTENT

Supporting Information

The Supporting Information is available free of charge at https://pubs.acs.org/doi/10.1021/acs.jpcb.1c10662.

> Mass density for scaled charge, full charge, and polarizable systems; full list of force field parameters; linear fitting of the mean square displacement; details of the calculation of cohesive energy; radial distribution functions that are based on certain atoms on the imidazolium ring; hopping event analysis based on the neighboring frame method; and the self-van Hove function as a function of simulation time for the scaled charge system (PDF)

■ AUTHOR INFORMATION

Corresponding Author

Venkat Ganesan − *McKetta Department of Chemical Engineering, University of Texas at Austin, Austin, Texas 78712, United States;* orcid.org/0000-0003-3899-5843; Email: venkat@che.utexas.edu

Authors

Zidan Zhang − *McKetta Department of Chemical Engineering, University of Texas at Austin, Austin, Texas 78712, United States;* orcid.org/0000-0002-6909-8742

Everett Zofchak − *McKetta Department of Chemical Engineering, University of Texas at Austin, Austin, Texas 78712, United States*

Jakub Krajniak − *Independent Researcher, 61-631 Poznan, Poland;* orcid.org/0000-0001-9372-6975

Complete contact information is available at: https://pubs.acs.org/10.1021/acs.jpcb.1c10662

Notes

The authors declare no competing financial interest.

■ ACKNOWLEDGMENTS

The authors thank Jesse G. McDaniel for insightful feedback and guidance on the cohesive energy and charge oscillation discussed herein. Our work on the topic of ion transport in polymer electrolytes has been generously supported by grants from the Robert A. Welch Foundation (grant F1599) and the National Science Foundation (DMR-1721512). The authors acknowledge the Texas Advanced Computing Center (TACC) for the generous allocation of computing resources. This material is based upon work supported by a National Science Foundation Graduate Research Fellowship under grant no. 000392968.

■ REFERENCES

(1) Winter, M.; Barnett, B.; Xu, K. Before Li Ion Batteries. *Chem. Rev.* **2018**, *118*, 11433−11456.

(2) Shen, X.; Zhang, X.-Q.; Ding, F.; Huang, J.-Q.; Xu, R.; Chen, X.; Yan, C.; Su, F.-Y.; Chen, C.-M.; Liu, X.; et al. Advanced Electrode Materials in Lithium Batteries: Retrospect and Prospect. *Energy Material Advances* **2021**, *2021*, 1205324.

(3) George, C. The coming electric vehicle transformation. *Science* **2019**, *366*, 422−424.

(4) Liang, Y.; Zhao, C.-Z.; Yuan, H.; Chen, Y.; Zhang, W.; Huang, J.-Q.; Yu, D.; Liu, Y.; Titirici, M.-M.; Chueh, Y.-L.; et al. A review of rechargeable batteries for portable electronic devices. *InfoMat* **2019**, *1*, 6−32.

(5) Ganesan, V. Ion transport in polymeric ionic liquids: recent developments and open questions. *Molecular Systems Design & Engineering* **2019**, *4*, 280−293.

(6) Lee, J. Z.; Wynn, T. A.; Schroeder, M. A.; Alvarado, J.; Wang, X.; Xu, K.; Meng, Y. S. Cryogenic Focused Ion Beam Characterization of Lithium Metal Anodes. *ACS Energy Letters* **2019**, *4*, 489−493.

(7) Xu, W.; Wang, J.; Ding, F.; Chen, X.; Nasybulin, E.; Zhang, Y.; Zhang, J.-G. Lithium metal anodes for rechargeable batteries. *Energy Environ. Sci.* **2014**, *7*, 513−537.

(8) Zachman, M. J.; Tu, Z.; Choudhury, S.; Archer, L. A.; Kourkoutis, L. F. Cryo-STEM mapping of solid−liquid interfaces and dendrites in lithium-metal batteries. *Nature* **2018**, *560*, 345−349.

(9) Austen Angell, C. Concepts and conflicts in polymer electrolytes: The search for ion mobility. *Electrochim. Acta* **2019**, *313*, 205−210.

(10) Mogurampelly, S.; Borodin, O.; Ganesan, V. Computer Simulations of Ion Transport in Polymer Electrolyte Membranes. *Annu. Rev. Chem. Biomol. Eng.* **2016**, *7*, 349−371.

(11) Mecerreyes, D.; Porcarelli, L.; Casado, N. Innovative Polymers for Next-Generation Batteries. *Macromol. Chem. Phys.* **2020**, *221*, 1900490.

(12) Forsyth, M.; Porcarelli, L.; Wang, X.; Goujon, N.; Mecerreyes, D. Innovative Electrolytes Based on Ionic Liquids and Polymers for Next-Generation Solid-State Batteries. *Acc. Chem. Res.* **2019**, *52*, 686−694.

(13) Eshetu, G. G.; Mecerreyes, D.; Forsyth, M.; Zhang, H.; Armand, M. Polymeric ionic liquids for lithium-based rechargeable batteries. *Molecular Systems Design & Engineering* **2019**, *4*, 294−309.
(14) Matsumi, N.; Sugai, K.; Miyake, M.; Ohno, H. Polymerized Ionic Liquids via Hydroboration Polymerization as Single Ion Conductive Polymer Electrolytes. *Macromolecules* **2006**, *39*, 6924−6927.
(15) Mecerreyes, D. Polymeric ionic liquids: Broadening the properties and applications of polyelectrolytes. *Prog. Polym. Sci.* **2011**, *36*, 1629−1648.
(16) Kim, O.; Kim, S. Y.; Lee, J.; Park, M. J. Building Less Tortuous Ion-Conduction Pathways Using Block Copolymer Electrolytes with a Well-Defined Cubic Symmetry. *Chem. Mater.* **2016**, *28*, 318−325.
(17) Ohno, H.; Ito, K. Room-Temperature Molten Salt Polymers as a Matrix for Fast Ion Conduction. *Chem. Lett.* **1998**, *27*, 751−752.
(18) Ohno, H. Molten salt type polymer electrolytes. *Electrochim. Acta* **2001**, *46*, 1407−1411.
(19) Yuan, J.; Mecerreyes, D.; Antonietti, M. Poly(ionic liquid)s: An update. *Prog. Polym. Sci.* **2013**, *38*, 1009−1036.
(20) Choi, J.-H.; Ye, Y.; Elabd, Y. A.; Winey, K. I. Network Structure and Strong Microphase Separation for High Ion Conductivity in Polymerized Ionic Liquid Block Copolymers. *Macromolecules* **2013**, *46*, 5290−5300.
(21) Shaplov, A. S.; Ponkratov, D. O.; Aubert, P.-H.; Lozinskaya, E. I.; Plesse, C.; Vidal, F.; Vygodskii, Y. S. A first truly all-solid state organic electrochromic device based on polymeric ionic liquids. *Chem. Commun.* **2014**, *50*, 3191−3193.
(22) Yu, Y.; Lu, F.; Sun, N.; Wu, A.; Pan, W.; Zheng, L. Single lithium-ion polymer electrolytes based on poly(ionic liquid)s for lithium-ion batteries. *Soft Matter* **2018**, *14*, 6313−6319.
(23) Huang, T.; Long, M.-C.; Wu, G.; Wang, Y.-Z.; Wang, X.-L. Poly(ionic liquid)-Based Hybrid Hierarchical Free-Standing Electrolytes with Enhanced Ion Transport and Fire Retardancy Towards Long-Cycle-Life and Safe Lithium Batteries. *ChemElectroChem.* **2019**, *6*, 3674−3683.
(24) Schauser, N. S.; Seshadri, R.; Segalman, R. A. Multivalent ion conduction in solid polymer systems. *Mol. Syst. Des. Eng.* **2019**, *4*, 263−279.
(25) Wang, X.; Kerr, R.; Chen, F.; Goujon, N.; Pringle, J. M.; Mecerreyes, D.; Forsyth, M.; Howlett, P. C. Toward High-Energy-Density Lithium Metal Batteries: Opportunities and Challenges for Solid Organic Electrolytes. *Adv. Mater.* **2020**, *32*, 1905219.
(26) Mogurampelly, S.; Keith, J. R.; Ganesan, V. Mechanisms Underlying Ion Transport in Polymerized Ionic Liquids. *J. Am. Chem. Soc.* **2017**, *139*, 9511−9514.
(27) Keith, J. R.; Mogurampelly, S.; Aldukhi, F.; Wheatle, B. K.; Ganesan, V. Influence of molecular weight on ion-transport properties of polymeric ionic liquids. *Phys. Chem. Chem. Phys.* **2017**, *19*, 29134−29145.
(28) Keith, J. R.; Rebello, N. J.; Cowen, B. J.; Ganesan, V. Influence of Counterion Structure on Conductivity of Polymerized Ionic Liquids. *ACS Macro Lett.* **2019**, *8*, 387−392.
(29) Keith, J. R.; Ganesan, V. Ion transport in backbone-embedded polymerized ionic liquids. *J. Chem. Phys.* **2019**, *151*, 124902.
(30) Zhang, Z.; Krajniak, J.; Keith, J. R.; Ganesan, V. Mechanisms of Ion Transport in Block Copolymeric Polymerized Ionic Liquids. *ACS Macro Lett.* **2019**, *8*, 1096−1101.
(31) Zhang, Z.; Krajniak, J.; Ganesan, V.; Multiscale, A. A Multiscale Simulation Study of Influence of Morphology on Ion Transport in Block Copolymeric Ionic Liquids. *Macromolecules* **2021**, *54*, 4997−5010.
(32) Mogurampelly, S.; Ganesan, V. Ion Transport in Polymerized Ionic Liquid−Ionic Liquid Blends. *Macromolecules* **2018**, *51*, 9471−9483.
(33) Keith, J. R.; Ganesan, V. Ion transport mechanisms in salt-doped polymerized zwitterionic electrolytes. *J. Polym. Sci.* **2020**, *58*, 578−588.
(34) Zhang, Z.; Nasrabadi, A. T.; Aryal, D.; Ganesan, V. Mechanisms of Ion Transport in Lithium Salt-Doped Polymeric Ionic Liquid Electrolytes. *Macromolecules* **2020**, *53*, 6995−7008.
(35) Zhang, Z.; Lin, D.; Ganesan, V. Mechanisms of ion transport in lithium salt-doped polymeric ionic liquid electrolytes at higher salt concentrations. *J. Polym. Sci.* **2022**, *60*, 199−213.
(36) Zhang, Z.; Wheatle, B. K.; Krajniak, J.; Keith, J. R.; Ganesan, V. Ion Mobilities, Transference Numbers, and Inverse Haven Ratios of Polymeric Ionic Liquids. *ACS Macro Lett.* **2020**, *9*, 84−89.
(37) Bhargava, B. L.; Balasubramanian, S. Refined potential model for atomistic simulations of ionic liquid [bmim][PF6]. *J. Chem. Phys.* **2007**, *127*, 114510.
(38) Molinari, N.; Kozinsky, B. Chelation-Induced Reversal of Negative Cation Transference Number in Ionic Liquid Electrolytes. *J. Phys. Chem. B* **2020**, *124*, 2676−2684.
(39) Lemkul, J. A.; Huang, J.; Roux, B.; MacKerell, A. D. An Empirical Polarizable Force Field Based on the Classical Drude Oscillator Model: Development History and Recent Applications. *Chem. Rev.* **2016**, *116*, 4983−5013.
(40) Lemkul, J. A.; MacKerell, A. D., Jr. Polarizable force field for RNA based on the classical drude oscillator. *J. Comput. Chem.* **2018**, *39*, 2624−2646.
(41) Jing, Z.; Liu, C.; Cheng, S. Y.; Qi, R.; Walker, B. D.; Piquemal, J.-P.; Ren, P. Polarizable Force Fields for Biomolecular Simulations: Recent Advances and Applications. *Annual Review of Biophysics* **2019**, *48*, 371−394.
(42) Gudla, H.; Zhang, C.; Brandell, D. Effects of Solvent Polarity on Li-ion Diffusion in Polymer Electrolytes: An All-Atom Molecular Dynamics Study with Charge Scaling. *J. Phys. Chem. B* **2020**, *124*, 8124−8131.
(43) Chen, X.; Hou, L.; Wei, X.; Bedrov, D. Transport Properties of Waxy Crude Oil: A Molecular Dynamics Simulation Study. *ACS omega* **2020**, *5*, 18557−18564.
(44) Dong, D.; Choudhary, A.; Bedrov, D. Coupling−Decoupling Transition between Li+ Transport and Segmental Relaxation in Solid Electrolytes. *ACS Applied Materials* **2020**, *2*, 5358−5364.
(45) Di Pasquale, N.; Elliott, J. D.; Hadjidoukas, P.; Carbone, P. Dynamically Polarizable Force Fields for Surface Simulations via Multi-output Classification Neural Networks. *J. Chem. Theory Comput.* **2021**, *17*, 4477−4485.
(46) Chen, P.; Vorobyov, I.; Roux, B.; Allen, T. W. Molecular Dynamics Simulations Based on Polarizable Models Show that Ion Permeation Interconverts between Different Mechanisms as a Function of Membrane Thickness. *J. Phys. Chem. B* **2021**, *125*, 1020−1035.
(47) Mitroy, J.; Safronova, M. S.; Clark, C. W. Theory and applications of atomic and ionic polarizabilities. *Journal of Physics B: Atomic, Molecular and Optical Physics* **2010**, *43*, 202001.
(48) Bedrov, D.; Piquemal, J.-P.; Borodin, O.; MacKerell, A. D.; Roux, B.; Schröder, C. Molecular Dynamics Simulations of Ionic Liquids and Electrolytes Using Polarizable Force Fields. *Chem. Rev.* **2019**, *119*, 7940−7995.
(49) Ren, P.; Ponder, J. W. Polarizable Atomic Multipole Water Model for Molecular Mechanics Simulation. *J. Phys. Chem. B* **2003**, *107*, 5933−5947.
(50) Jing, Z.; Liu, C.; Ren, P. Advanced Electrostatic Model for Monovalent Ions Based on Ab Initio Energy Decomposition. *J. Chem. Inf. Model.* **2021**, *61*, 2806−2817.
(51) Wang, L.-P.; Head-Gordon, T.; Ponder, J. W.; Ren, P.; Chodera, J. D.; Eastman, P. K.; Martinez, T. J.; Pande, V. S. Systematic Improvement of a Classical Molecular Model of Water. *J. Phys. Chem. B* **2013**, *117*, 9956−9972.
(52) Loco, D.; Polack, É.; Caprasecca, S.; Lagardère, L.; Lipparini, F.; Piquemal, J.-P.; Mennucci, B. A QM/MM Approach Using the AMOEBA Polarizable Embedding: From Ground State Energies to Electronic Excitations. *J. Chem. Theory Comput.* **2016**, *12*, 3654−3661.
(53) Loco, D.; Lagardère, L.; Caprasecca, S.; Lipparini, F.; Mennucci, B.; Piquemal, J.-P. Hybrid QM/MM Molecular Dynamics with AMOEBA Polarizable Embedding. *J. Chem. Theory Comput.* **2017**, *13*, 4025−4033.
(54) Schmollngruber, M.; Lesch, V.; Schröder, C.; Heuer, A.; Steinhauser, O. Comparing induced point-dipoles and Drude oscillators. *Phys. Chem. Chem. Phys.* **2015**, *17*, 14297−14306.

https://doi.org/10.1021/acs.jpcb.1c10662
J. Phys. Chem. B 2022, 126, 2583−2592

(55) Patel, S.; Brooks, C. L. Fluctuating charge force fields: recent developments and applications from small molecules to macromolecular biological systems. *Mol. Simul.* **2006**, *32*, 231−249.
(56) Olano, L. R.; Rick, S. W. Fluctuating charge normal modes: An algorithm for implementing molecular dynamics simulations with polarizable potentials. *J. Comput. Chem.* **2005**, *26*, 699−707.
(57) Zhao, D.-X.; Liu, C.; Wang, F.-F.; Yu, C.-Y.; Gong, L.-D.; Liu, S.-B.; Yang, Z.-Z. Development of a Polarizable Force Field Using Multiple Fluctuating Charges per Atom. *J. Chem. Theory Comput.* **2010**, *6*, 795−804.
(58) Chen, J.; Hundertmark, D.; Martínez, T. J. A unified theoretical framework for fluctuating-charge models in atom-space and in bond-space. *J. Chem. Phys.* **2008**, *129*, 214113.
(59) Cavalcante, A. d. O.; Ribeiro, M. C. C.; Skaf, M. S. Polarizability effects on the structure and dynamics of ionic liquids. *J. Chem. Phys.* **2014**, *140*, 144108.
(60) Wu, Y.; Li, Y.; Hu, N.; Hong, M. The electronegativity equalization method fused with molecular mechanics: a fluctuating charge and flexible body potential function for [Emim][Gly] ionic liquids. *Phys. Chem. Chem. Phys.* **2014**, *16*, 2674−2685.
(61) Lamoureux, G.; Roux, B. Modeling induced polarization with classical Drude oscillators: Theory and molecular dynamics simulation algorithm. *J. Chem. Phys.* **2003**, *119*, 3025−3039.
(62) Schröder, C.; Steinhauser, O. Simulating polarizable molecular ionic liquids with Drude oscillators. *J. Chem. Phys.* **2010**, *133*, 154511.
(63) Yu, H.; Whitfield, T. W.; Harder, E.; Lamoureux, G.; Vorobyov, I.; Anisimov, V. M.; MacKerell, A. D.; Roux, B. Simulating Monovalent and Divalent Ions in Aqueous Solution Using a Drude Polarizable Force Field. *J. Chem. Theory Comput.* **2010**, *6*, 774−786.
(64) Chowdhary, J.; Harder, E.; Lopes, P. E. M.; Huang, L.; MacKerell, A. D.; Roux, B. A Polarizable Force Field of Dipalmitoylphosphatidylcholine Based on the Classical Drude Model for Molecular Dynamics Simulations of Lipids. *J. Phys. Chem. B* **2013**, *117*, 9142−9160.
(65) Zhang, Q.; Xu, R.; Kan, D.; He, X. Molecular dynamics simulation of electric-field-induced self-assembly of diblock copolymers. *J. Chem. Phys.* **2016**, *144*, 234901.
(66) Lin, F.-Y.; Lopes, P. E. M.; Harder, E.; Roux, B.; MacKerell, A. D. Polarizable Force Field for Molecular Ions Based on the Classical Drude Oscillator. *J. Chem. Inf. Model.* **2018**, *58*, 993−1004.
(67) Wang, H.; DeFever, R. S.; Zhang, Y.; Wu, F.; Roy, S.; Bryantsev, V. S.; Margulis, C. J.; Maginn, E. J. Comparison of fixed charge and polarizable models for predicting the structural, thermodynamic, and transport properties of molten alkali chlorides. *J. Chem. Phys.* **2020**, *153*, 214502.
(68) McDaniel, J. G.; Yethiraj, A. Influence of Electronic Polarization on the Structure of Ionic Liquids. *J. Phys. Chem. Lett.* **2018**, *9*, 4765−4770.
(69) Goloviznina, K.; Canongia Lopes, J. N.; Costa Gomes, M.; Pádua, A. A. H. Transferable, Polarizable Force Field for Ionic Liquids. *J. Chem. Theory Comput.* **2019**, *15*, 5858−5871.
(70) Jeong, K.-j.; McDaniel, J. G.; Yethiraj, A.; Transferable, A. A Transferable Polarizable Force Field for Urea Crystals and Aqueous Solutions. *J. Phys. Chem. B* **2020**, *124*, 7475−7483.
(71) Klajmon, M.; Červinka, C. Does Explicit Polarizability Improve Simulations of Phase Behavior of Ionic Liquids? *J. Chem. Theory Comput.* **2021**, *17*, 6225−6239.
(72) Jorgensen, W. L.; Maxwell, D. S.; Tirado-Rives, J. Development and Testing of the OPLS All-Atom Force Field on Conformational Energetics and Properties of Organic Liquids. *J. Am. Chem. Soc.* **1996**, *118*, 11225−11236.
(73) Chaban, V. Polarizability versus mobility: atomistic force field for ionic liquids. *Phys. Chem. Chem. Phys.* **2011**, *13*, 16055−16062.
(74) Martínez, L.; Andrade, R.; Birgin, E. G.; Martínez, J. M. PACKMOL: A package for building initial configurations for molecular dynamics simulations. *J. Comput. Chem.* **2009**, *30*, 2157−2164.
(75) Larsen, G. S.; Lin, P.; Hart, K. E.; Colina, C. M. Molecular Simulations of PIM-1-like Polymers of Intrinsic Microporosity. *Macromolecules* **2011**, *44*, 6944−6951.
(76) Hart, K. E.; Abbott, L. J.; McKeown, N. B.; Colina, C. M. Toward Effective CO2/CH4 Separations by Sulfur-Containing PIMs via Predictive Molecular Simulations. *Macromolecules* **2013**, *46*, 5371−5380.
(77) Plimpton, S. Fast Parallel Algorithms for Short-Range Molecular Dynamics. *J. Comput. Phys.* **1995**, *117*, 1−19.
(78) Goloviznina, K.; Gong, Z.; Costa Gomes, M. F.; Pádua, A. A. H. Extension of the CL&Pol Polarizable Force Field to Electrolytes, Protic Ionic Liquids, and Deep Eutectic Solvents. *J. Chem. Theory Comput.* **2021**, *17*, 1606−1617.
(79) Heid, E.; Heindl, M.; Dienstl, P.; Schröder, C. Additive polarizabilities of halides in ionic liquids and organic solvents. *J. Chem. Phys.* **2018**, *149*, 44302.
(80) Thole, B. T. Molecular polarizabilities calculated with a modified dipole interaction. *Chem. Phys.* **1981**, *59*, 341−350.
(81) Dequidt, A.; Devémy, J.; Pádua, A. A. H. Thermalized Drude Oscillators with the LAMMPS Molecular Dynamics Simulator. *J. Chem. Inf. Model.* **2016**, *56*, 260−268.
(82) Son, C. Y.; McDaniel, J. G.; Cui, Q.; Yethiraj, A. Proper Thermal Equilibration of Simulations with Drude Polarizable Models: Temperature-Grouped Dual-Nosé−Hoover Thermostat. *J. Phys. Chem. Lett.* **2019**, *10*, 7523−7530.
(83) Son, C. Y.; McDaniel, J. G.; Schmidt, J. R.; Cui, Q.; Yethiraj, A. First-Principles United Atom Force Field for the Ionic Liquid BMIM +BF4−: An Alternative to Charge Scaling. *J. Phys. Chem. B* **2016**, *120*, 3560−3568.
(84) McDaniel, J. G.; Yethiraj, A. Understanding the Properties of Ionic Liquids: Electrostatics, Structure Factors, and Their Sum Rules. *J. Phys. Chem. B* **2019**, *123*, 3499−3512.
(85) Doherty, B.; Zhong, X.; Gathiaka, S.; Li, B.; Acevedo, O. Revisiting OPLS Force Field Parameters for Ionic Liquid Simulations. *J. Chem. Theory Comput.* **2017**, *13*, 6131−6145.
(86) Liu, H.; Luo, X.; Sokolov, A. P.; Paddison, S. J. Quantitative Evidence of Mobile Ion Hopping in Polymerized Ionic Liquids. *J. Phys. Chem. B* **2021**, *125*, 372−381.
(87) Shen, K.-H.; Hall, L. M. Ion Conductivity and Correlations in Model Salt-Doped Polymers: Effects of Interaction Strength and Concentration. *Macromolecules* **2020**, *53*, 3655−3668.
(88) Fong, K. D.; Self, J.; Diederichsen, K. M.; Wood, B. M.; McCloskey, B. D.; Persson, K. A. Ion Transport and the True Transference Number in Nonaqueous Polyelectrolyte Solutions for Lithium Ion Batteries. *ACS Central Science* **2019**, *5*, 1250−1260.
(89) Fong, K. D.; Self, J.; McCloskey, B. D.; Persson, K. A. Onsager Transport Coefficients and Transference Numbers in Polyelectrolyte Solutions and Polymerized Ionic Liquids. *Macromolecules* **2020**, *53*, 9503−9512.

https://doi.org/10.1021/acs.jpcb.1c10662
J. Phys. Chem. B 2022, 126, 2583−2592